frontiers | Frontiers in Earth Science

TYPE Review
PUBLISHED 18 December 2024
DOI 10.3389/feart.2024.1492024

OPEN ACCESS

EDITED BY
Rizwan Rasheed,
Government College University, Pakistan

REVIEWED BY
Zhengzheng Cao,
Henan Polytechnic University, China
Steven J. Schatzel,
Centers for Disease Control and Prevention (CDC), United States
Qaiser Khan,
Government College University, Pakistan

*CORRESPONDENCE
Junhui Fu,
fuphy@163.com

RECEIVED 06 September 2024
ACCEPTED 27 November 2024
PUBLISHED 18 December 2024

CITATION
Fu J, Wen G, Zhang B, Sun H, Li R and Liu J (2024) Optimization design of stress relief coalbed methane surface well in a high-gas mine.
Front. Earth Sci. 12:1492024.
doi: 10.3389/feart.2024.1492024

Optimization design of stress relief coalbed methane surface well in a high-gas mine

Junhui Fu[1]*, Guangcai Wen[1], Bichuan Zhang[2], Haitao Sun[1], Rifu Li[1] and Jiaqi Liu[2]

[1]Gas Research Branch, China Coal Technology Engineering Group Chongqing Research Institute, Chongqing, China, [2]Key-Laboratory of In-Situ Properties-Modified Mining of Ministry of Education, Taiyuan University of Technology, Taiyuan, China

Coalbed methane drainage through surface wells has become increasingly important in high-gas mines. Surface wells are prone to different types of deformations and failures owing to mining-induced effects. In this paper, a displacement and deformation model was established for the overlying strata. Three forms of deformation and failure of the surface well casing was proposed, namely shearing, stretching, and uneven extrusion. Moreover, the mathematical model functions for the S-type shear deformation, delamination tensile deformation, and non-uniform extrusion of the surface well were established. In the Shanxi Coal Group Yue Cheng Mine, coalbed methane drainage at the surface well was conducted on the mining-affected area to achieve good effects. The YCCD-04 well without a local protective device was deformed and damaged, and the dynamic deformation and failure of the surface well was detected using a well imager. The YCCD-02 surface well with a local protective device showed good mining and gas drainage, which verified the effectiveness of the local protective device; the coalbed methane drainage time of this surface well was 35 months, and the cumulative coalbed methane drainage volume extracted was 1.3×10^7 m^3. Simultaneously, the problem of gas control in the working face was solved, thereby ensuring the safety of coal mining and achieving good social as well as economic benefits.

KEYWORDS

surface well deformation, coalbed methane drainage, overlying strata movement, safety protection, surface well structure

1 Introduction

According to the accident inquiry system of the National Coal Mine Safety Supervision Bureau of China, 76 gas outburst accidents have occurred in recent years, resulting in the deaths of 608 people and injuring about 105 people; these statistics account for 48.4% of the total number of accidents, 57.7% of the total number of deaths, and 68.2% of the total number of injuries, respectively. Therefore, coal mine gas disasters are rather serious and pose serious threats to mine safety production (Guo et al., 2018; Li et al., 2019; Zhuo et al., 2024). Coalbed methane (CBM) is a high-quality clean source of energy as well as a good industrial, chemical, power generation, and residential fuel (Buzek et al., 2022; Jha et al., 2022; Wang et al., 2019; Zhao et al., 2021; Zhou et al., 2020). Moreover, CBM drainage is important for safe production in coal mines and utilization

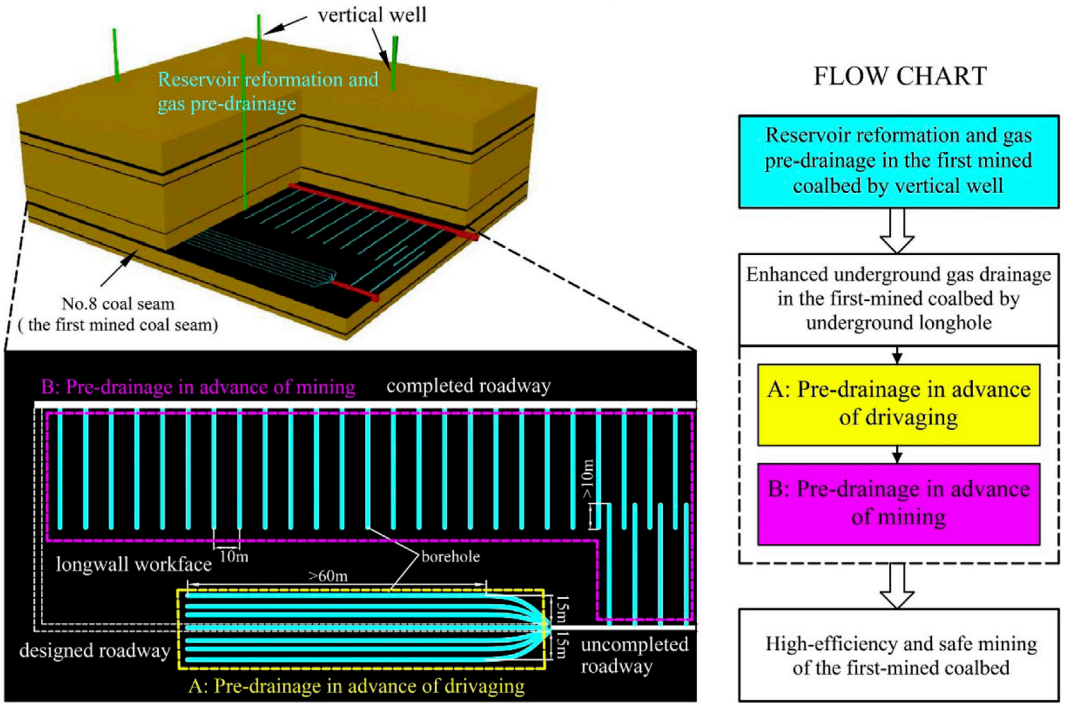

FIGURE 1
Schematic view of the underground intensified gas drainage (Kong et al., 2014).

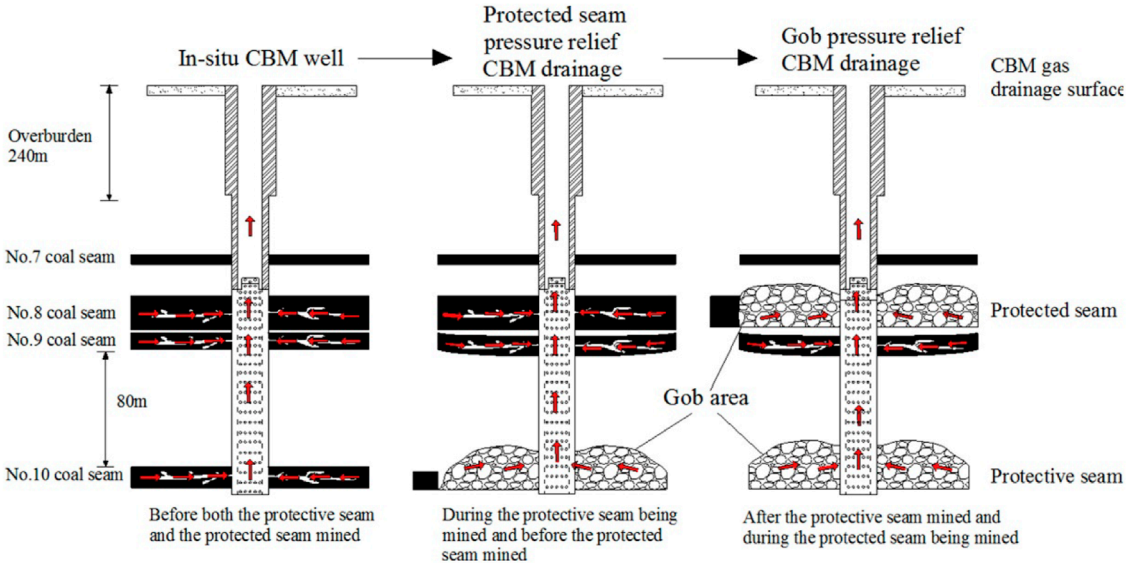

FIGURE 2
Different stages of pressure relief during coalbed methane (CBM) extraction at the multipurpose well (Wang et al., 2014).

of gaseous resources (Joshi et al., 2023; Kishor et al., 2023; Ponnudurai et al., 2022; Ye et al., 2023).

Sang et al. (2010) summarized the statuses of engineering practices, technologies, and research related to stress relief CBM drainage using surface wells in China. In high-gas mining areas characterized by heavily sheared coals with relatively low permeabilities, such as the Huainan, Huaibei, and Tiefa regions, stress relief CBM drainage through surface wells has been implemented successfully and achieved broad acceptance as a CBM exploitation technology. CBM drainage technologies mainly include surface fracturing of the original coal seam and underground mining (Figure 1). CBM drainage through surface wells takes full advantage of the mining and unloading effects (Qu et al., 2016); it is an important method of obtaining coal mine gas, which is a good

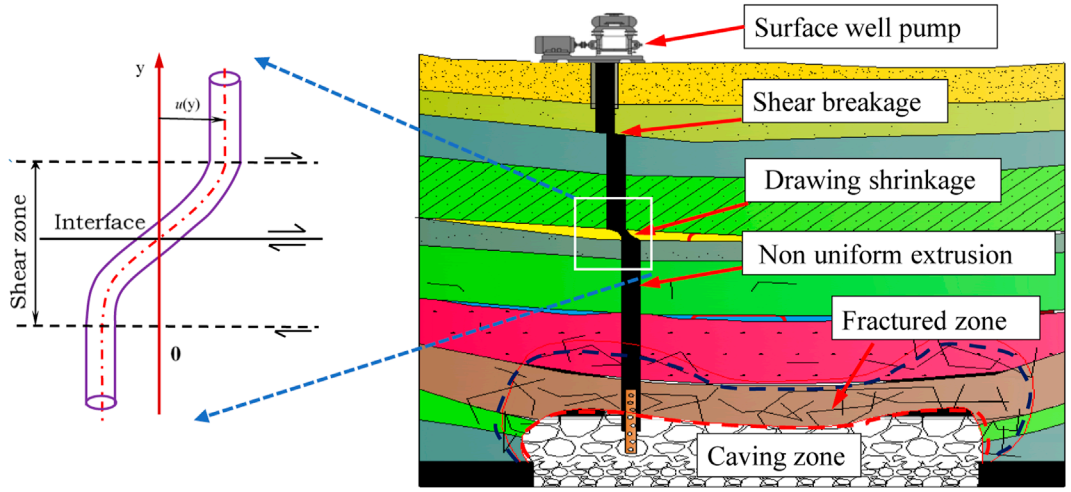

FIGURE 3
Deformation mode of the surface well in the mining area and "S"-shaped model of casing shear deformation.

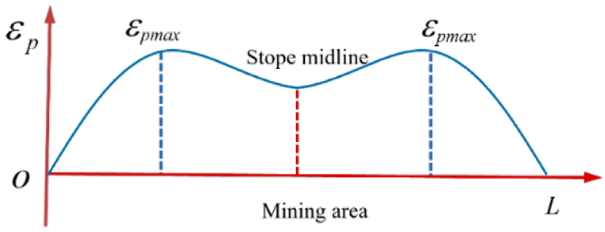

FIGURE 4
Horizontal distribution of the shear deformation at ground drilling.

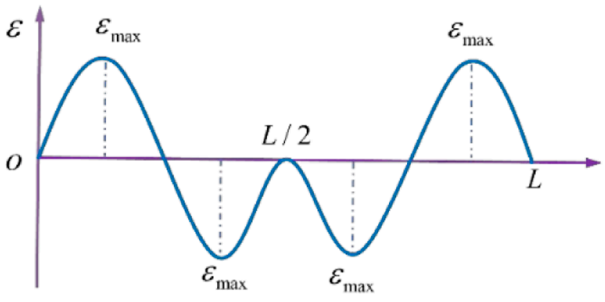

FIGURE 5
Rock layer strain distribution curve for full subsidence (positive tensile strain, while the compressive strain should be negative).

solution to the gas problems. With the advancement of the working face, the overburden of the stope is affected by mining. Pushing the coal mining face through the well achieves the purposes of coal-mining-face gas management and CBM drainage (Newman et al., 2017; Ran et al., 2023; Zhang et al., 2020a; Zhang et al., 2024).

Rock thickness and lithological combination together control the failure of the wellbore inside the rock formation. The combination of hard and soft lithologies is prone to axial tensile and compressive failures caused by separation from the bed; such combination can easily result in shear failure in the weak structural plane, and the middle part of the soft rock layer with thick upper and thin lower structures as well as soft upper and hard lower structures is prone to combined failure. High mining speed and rapid advancement can also exacerbate the above types of damage. Therefore, it is important to study CBM drainage in the mining area. Many researchers have studied wellbore casing failure during the coal mining process in collapsed areas (Whittles et al., 2007); they analyzed the damage from the casing and the effects of the lithological parameters (Whittles et al., 2006). In France, an experimental method was used to study the failure characteristics of surrounding rocks, which showed that the principal stress on the well wall has important effects on the stability of the well (Chi et al., 2019; Ju et al., 2019; Zhang et al., 2021). The quantitative relationships between the geological well-failure characteristics and geostresses were used to initially obtain the relationships among different geostresses and deformations of the ground drills (Fu et al., 2020; Luan et al., 2020; Sun et al., 2022). Xu et al. (2011) found that the production and stability of the drainage wells were affected by deformation and damage of the overlying strata. The second distribution of the strata stress is caused by mining engineering; if the stress load is larger than the carrying capacity of the extraction well, then the gas production would be influenced by the drainage well that has been damaged by rock movements. Liu et al. (2005) regarded the overlying rock mass as a homogeneous medium and proposed the design requirement that the drilling hole diameter should be greater than the horizontal deformation of the rock mass. Ren et al. (2018) proposed that the main causes of failure of the surface gas extraction wells are the overburden separation, stress concentration, vertical fractures, and composite effects of the junction between the thick-flow sand layer and bedrock caused by mining; the main deformations and failures of the surface wells include tensile, extrusion, shear, and tensile-shear comprehensive failures; furthermore, the separation of the overburden from bottom

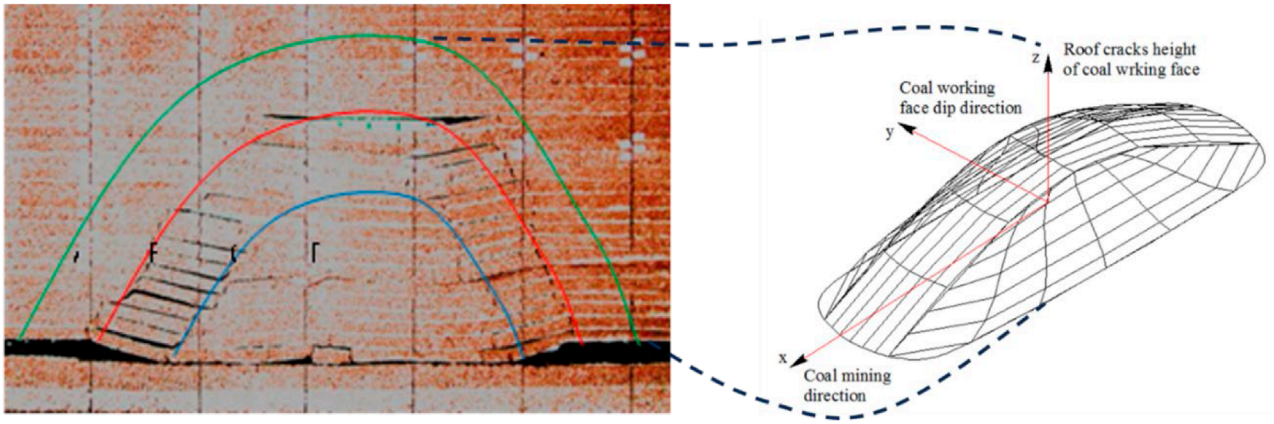

FIGURE 6
Elliptical morphology of the fissure.

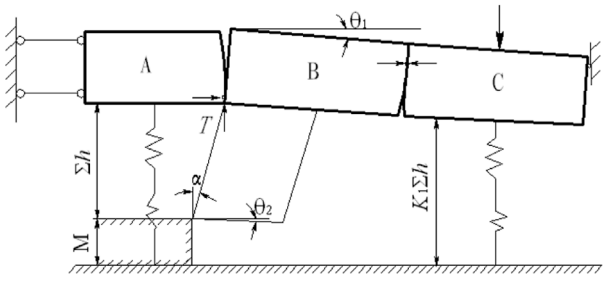

FIGURE 7
Overall mechanical model of the surrounding rock.

to top, stress concentration, and rock-layer breakage cause multiple deformations and failures in gas surface wells. Schatzel et al. (2012) discussed the relationships between changing reservoir conditions, longwall face position, and surface movements. Su et al. (2019) described the surface deformations and permeability changes in shale gas wells. Zhang et al. (2023) studied the casing deformations of shale gas wells in the longwall chain pillars.

In the present paper, a displacement and deformation model was established for the overlying strata to study the mining-induced effects on surface wells. Then, the surface well structure was designed to adapt to such mining-induced effects. In addition, the compromised region of the surface well was protected using well safety measures, such as antishearing, antitensile damage, and thick-walled rigid devices. Finally, the surface well in the Shanxi Coal Group Yue Cheng Mine was used as the case study to verify the proposed method.

2 Deformation and failure of the surface well in a mining area

When a coal seam is completely mined, the overlying strata will inevitably break and rotate. The surface wells for the CBM in the mining area will then be damaged by the rotation and sinking effects of the rock. When the overlying strata move and deform, shear deformations can easily occur between the rock boundaries of the stope and bedding separation deformation in the middle cover of the stope (Chen et al., 2022; Wang et al., 2020; Zhang et al., 2020b). It is easy to cut the casing at the boundary of the stope such that tensile shrinkage damage occurs in the overburden while non-uniform extrusion failure occurs in the combined rock beam, as shown in Figure 2.

2.1 Shear failure analysis of the surface well

Interlayer shear slip occurs in the overlying strata of the stope owing to mining-induced effects. The shear deformation from drilling occurs at the interface between the two strata within a certain area of the drilling axis; this deformation is similar to an "S" shape, as shown in Figure 3.

The S-shaped shear deformation model of the surface well is given by

$$\varepsilon_p = \frac{\frac{\pi u_p^2}{4a}\sin\left(\frac{4\pi y}{a}\right) + y}{\sqrt{0.125u_p^2\left[1-\cos\left(\frac{4\pi y}{a}\right)\right] + y^2}} - 1, \quad (1)$$

where ε_p is the deformation strain of the surface well; u_p is the rock displacement at the drilling location; a is twice the width of the shear zone, which is related to the physical and mechanical properties as well as the stress environment of the rock formation, and is the length along the casing in the shear zone.

According to Equation 1, during roof movement, the local minimum point of deformation occurs at the midpoint of the rock beam. Moreover, the shear deformation increases slowly at both ends of the rock beam and reaches the maximum value at the midpoint of the subsidence curve as well as at the deflection point of the rock beam. Consequently, the shear deformation reduces rapidly along the beam and drops to zero the end points of the rock beam. From the shear deformation analysis, the surface well should be positioned between the end of the rock beam and the inflection point, as shown in Figure 4.

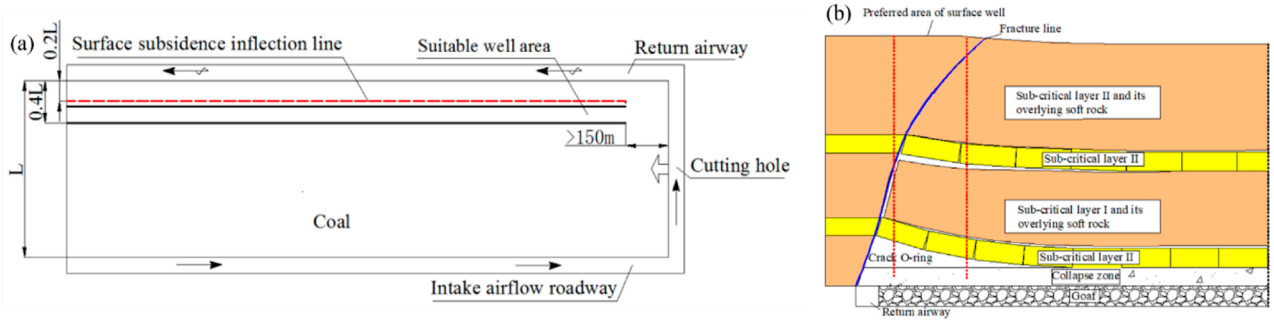

FIGURE 8
Schematic representation of the area suitable for surface wells within the mining area: **(A)** surface well layout plan; **(B)** surface well layout profile.

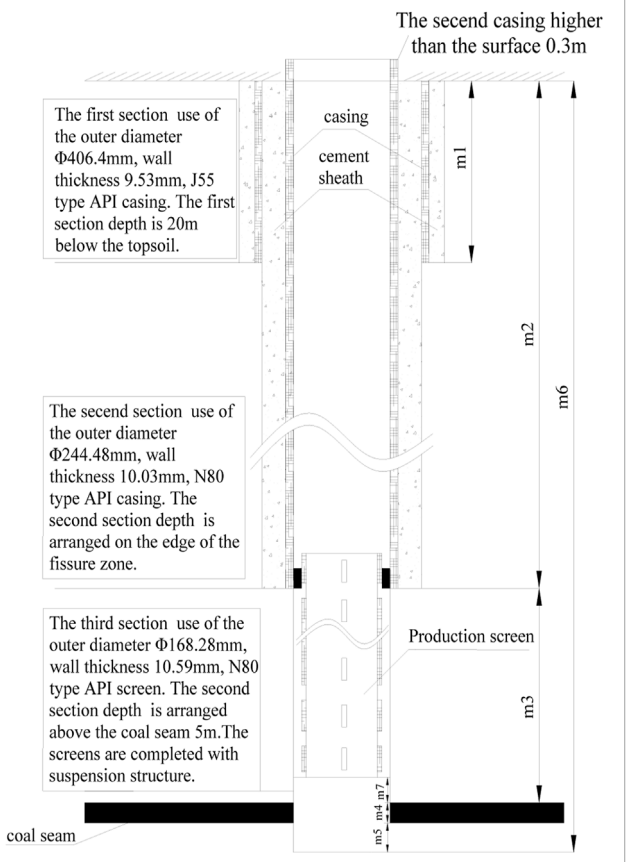

FIGURE 9
Structure of the surface well in the mining area.

2.2 Stretching deformation analysis of the surface well

During coal seam mining, the lower part of the key layer (or combination of key layers) in the overlying strata of the stope is prone to abscission layer displacement, as shown in Figure 5. Under the action of the abscission layer, the surface well casing produces tensile deformation followed by neck deformation. The layered tensile deformation is depicted in Figure 5.

The deformation of the rock itself is the root cause of the radial deformation of the casing. The rock beam structure satisfies the linear elastic relation $\sigma = E\varepsilon$. Moreover, the cross-sectional normal stress of the equivalent rock beam structure is given by the following (Equation 2):

$$\begin{cases} \varepsilon = -\dfrac{2\pi w_0}{r_Y^3} y(x - r_Y) e^{-\pi \frac{(x-r_Y)^2}{r_Y^2}} \\ \varepsilon^e = -\dfrac{2\pi w_0}{r_Y^3} y\left[(x - r_Y) e^{-\pi \frac{(x-r_Y)^2}{r_Y^2}} - (x - r_Y - l) e^{-\pi \frac{(x-r_Y-l)^2}{r_Y^2}}\right] \end{cases} \begin{matrix} (\text{Semi} - \text{infinite mining}) \\ (\text{Limited mining}) \end{matrix} \quad (2)$$

where w_0 is the maximum settlement displacement of the rock strata in the equivalent composite rock beam, which is related to the nature of the stratum and the mining process; r_Y is the upper surface depth of the rock as the base depth.

The deformation and distribution curves of the rock strata are symmetrically distributed about the midpoint of the rock beam. Moreover, the deformation reaches its maximum value near the fixed end of the beam at approximately $0.4r_Y$. The deformation profile of the rock beam along the neutral surface is shown in Figure 5.

3 Layout of the well location in the mining area

3.1 Determination of the surface well positions

Based on simulation of the overburden movements, the basic form of the mining fissure is obtained from the simulation test of coal mine excavation. The fracture field is divided into four zones as the unaffected area (zone A), supporting fracture area (zone B), fissure development area (zone C), and recompaction fissure area (zone D), as shown in Figure 6. According to the fracture form in Figure 6, it is observed that the vertical fractures in the direction of the coal seam are generally parabolic. From the spatial perspective, the fracture form is an approximately elliptical surface. By taking the center of the coal mining and dip directions as the origin, the model of the elliptical surface is established as shown in Figure 6.

The x-axis is the working face direction, the y-axis is the direction of the length of the working face, and the z-axis is the direction of the overlying rock fracture height. Furthermore, a is the length of the working face, l is the length of the main roof

TABLE 1 Parameters of the deflection protection equipment.

Outside diameter/mm	Inner diameter/mm	Length/mm	Maximum angle/°	Material type
300	220	487	3.5°	40Cr

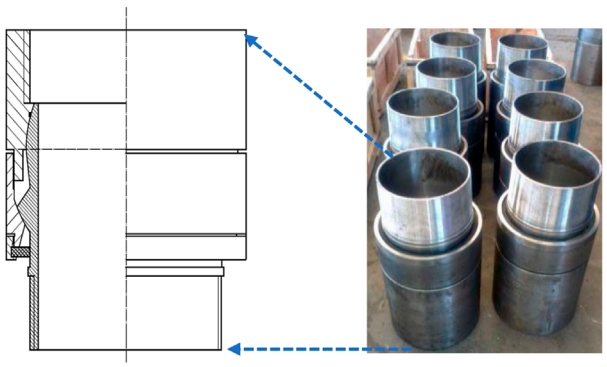

FIGURE 10
Assembly diagram and photograph of the deflection protection equipment.

TABLE 2 Parameters of the expansion protection equipment.

Outside diameter/mm	Inner diameter/mm	Length/mm	Elongation/°	Material type
300	220	940	+300 to −100	40Cr

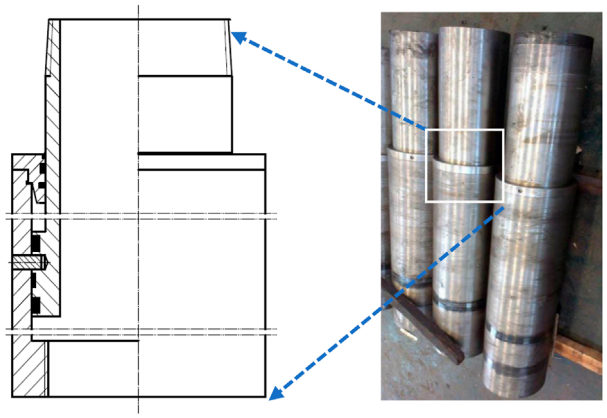

FIGURE 11
Assembly diagram and photograph of the expansion protection equipment.

TABLE 3 Parameters of the expansion protection equipment.

Wall thickness/mm	Length/mm	Outside diameter/mm	Inner diameter/mm	Material type
46	4,000	302	210	N80

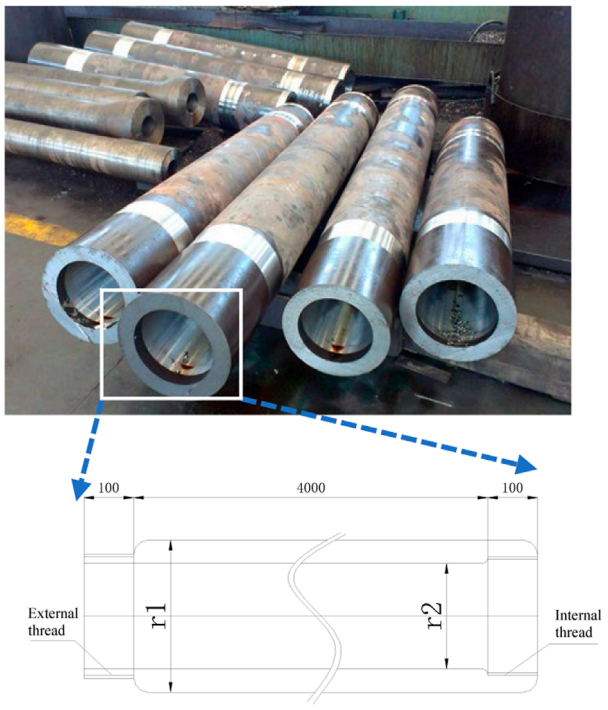

FIGURE 12
Assembly diagram and photograph of the thick-walled rigid protection equipment.

breaking rock, L is the distance advanced for the coal face, and h_0 is the fracture height of the mining overburden. Therefore, the general mathematical expression of the external elliptical surface is given by Equation 3

$$\frac{x^2}{\left(\frac{L}{2}\right)^2}+\frac{y^2}{\left(\frac{a}{2}\right)^2}=-z+h_0\frac{x^2}{\left(\frac{L}{2}\right)^2}+\frac{y^2}{\left(\frac{a}{2}\right)^2}=-z. \tag{3}$$

Moreover, the general mathematical expression of the inner elliptical surface is (Equation 4)

$$\frac{x^2}{\left(\frac{L}{2}-l\right)^2}+\frac{y^2}{\left(\frac{L}{2}-l\right)^2}=-z+h_0-l\frac{x^2}{\left(\frac{L}{2}-l\right)^2}+\frac{y^2}{\left(\frac{a}{2}-l\right)^2}=-z. \tag{4}$$

The inner elliptical surface is obtained from the length l (i.e., the block length of B) of the outer ellipse offset inwardly. The B blocks are formed around the area in contact with the

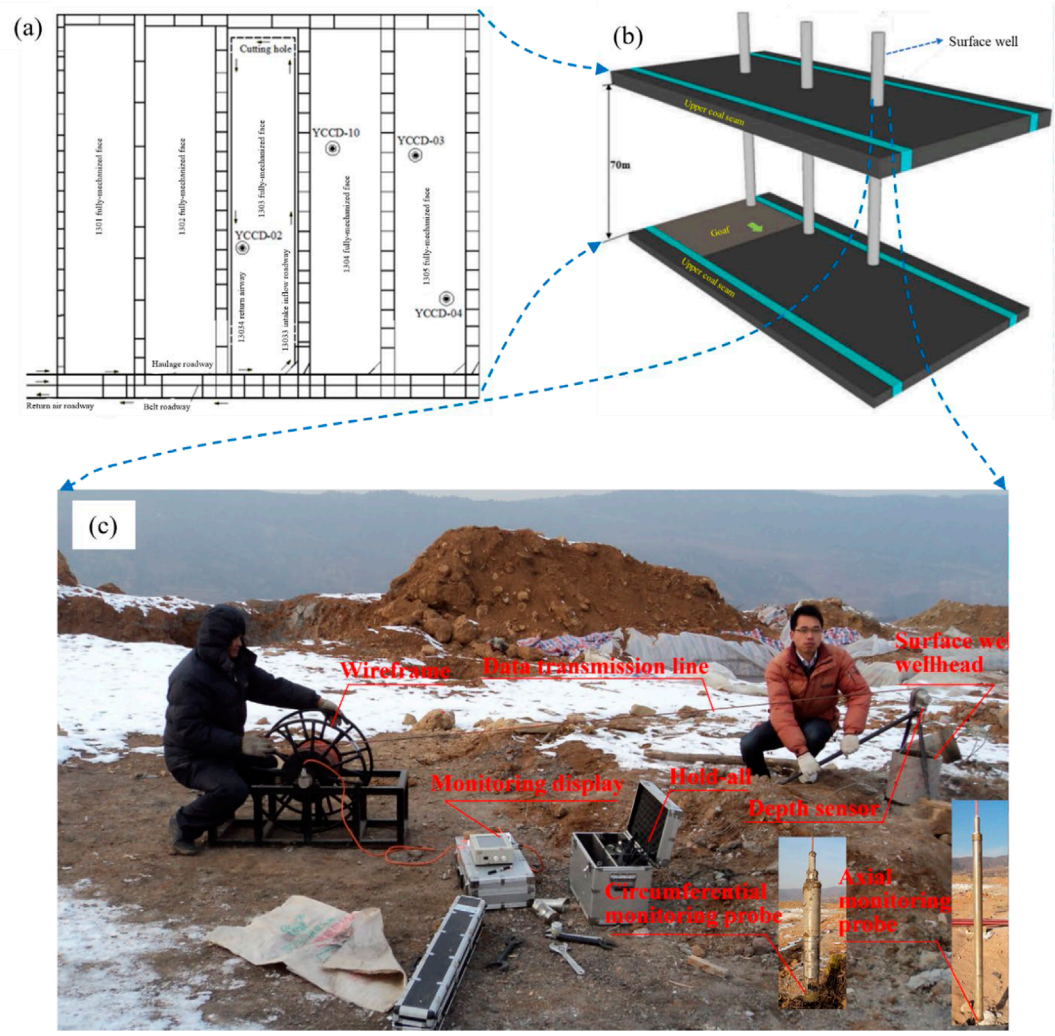

FIGURE 13
Steps of the surface well deformation monitoring in the Yuecheng Coal Mine: **(A)** locations of different working panels, **(B)** positions of the surface wells, and **(C)** detection site for surface well monitoring (Author pictured).

physical coal in the smoothed stabilization zone. A large number of separation cracks exist between the inner and outer ellipsoid surfaces, which is the main area of gas enrichment. The mechanical properties and morphology of the "masonry beam" structure are formed subsequent to the fracture of the old roof, as presented in Figure 7.

Therefore, the length l of the B rock block is mainly given by the following relationship (Equation 5):

$$l = \frac{M - \sum h(k-1)}{\tan \theta_1}, \tag{5}$$

where l is the length of the old roof broken rock (B block); M is the height of the top coal, where the top coal is the total thickness; Σh is the direct top thickness; k is the direct top compacted bulk coefficient; θ is the rotation angle of the main roof broken rock (B block).

Therefore, the mining effects of the surface well should be arranged in the area between the inner and outer ellipsoid surfaces, while the upper surface of the coal face constitutes the return airway side. Thus, the surface wells should be positioned close to the return airway side between the inner and outer ellipsoid surfaces.

3.2 Principle of surface well positioning in the mining area

The surface well positions in the coal mining area should be considered in favor of both the stability of the surface well structure and CBM extraction. The horizontal position of the surface well should be determined based on the fissure zone height of the overlying strata in the stope. The upper end of the production casing should be along the upper edge of the crack zone of the overlying strata, while the lower end of the production casing should be located in the caving zone (Zhang et al., 2022).

The surface wells should be positioned close to the return airway side between the inner and outer ellipsoid surfaces. From

TABLE 4 Well imager parameters.

Probe model	Parameter	Numerical value	Remarks
CXK-6T	Probe diameter	67 mm	Apply Φ25–Φ500 mm
	Probe length	800 mm	Explosion proof with coal safety certificate
	Probe pixel	1.34 million	
CXK-12T	Probe diameter	42 mm	Apply Φ25–Φ500 mm
	Probe length	1,200 mm	Explosion proof with coal safety certificate
	Probe pixel	13.00 million	

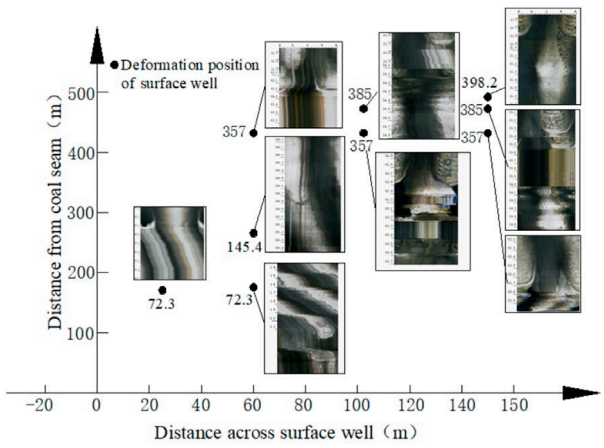

FIGURE 14
Monitoring results of the deformations in the YCCD-04 surface well.

the perspective of wellbore structure stability from the ground, the surface well should be located as far as possible from the maximum area of shear and delamination stretching. Moreover, the surface well should be located between the surface settlement and midline. The locations of the wells in the coal mining area are presented in Figure 8.

4 Design and safety protection of the surface well

4.1 Design of the surface well

Through the characteristics analyses of the drilling deformation and failure along with the characteristics of the gas field wells in the mining area, the surface wells of the mining area were arranged at 0.2–0.4 times the working distance of the working face. The surface well design was based on the specifications of "the code for design of surface vertical well for gas drainage in coal mining influence region" (NB/T 10365-2019). Moreover, the surface wells were optimized for mining-induced effects according to the deformation model in Section 3. The specific design of the well was as follows.

The first section was located in the bedrock at a depth of approximately 20 m, where the casing was of the J55-type API. The second section was located below the surface at the edge of the fissure zone with the N80-type casing and good shear performance, in addition to a portion of the local cementing measures during the second mining. The casing of the third section was used as the CBM drainage channel, and it was located in the coal seam at a depth of beyond 2–6 m. Moreover, the casing of the third section was designed to be suspended such that it was open and without cementing. The surface well structure design is as shown in Figure 9.

Qian et al. (2018) and Qian et al. (2003) analyzed the movement law of the overlying strata and showed that the bending moment is borne by small sections of each of the n layers of the composite beam according to the combined rock beam principle (Equation 6):

$$\frac{M_1}{E_1 J_1} = \frac{M_2}{E_2 J_2} = \cdots\cdots\cdots \frac{M_n}{E_n J_n}, \tag{6}$$

where M is the bending moment; E is the elastic modulus; J is the moment of inertia.

Thus, $(q_n)_1$ is calculated as Equation 7

$$(q_n)_1 = \frac{E_1 h_1^3 (\gamma_1 h_1 + \gamma_2 h_2 + \cdots\cdots\cdots \gamma_n h_n)}{E_1 h_1^3 + E_2 h_2^3 + \cdots\cdots\cdots E_n h_n^3}, \tag{7}$$

where $(q_n)_1$ is the total load when the formation affects the key layer; γ is the rock mass density; h is the thickness of the rock.

Therefore, the stress level of the strata (key layer) that mainly involves the bearing of the overburden is obtained, and the key layer of the overlying rock is seriously deformed before breakage of the rock mass; it is possible to install the antitension and antishear protection devices at the position of the largest deformation. In the overlying strata, the squeezing force of the composite rock beam in the key layer or combination of key layers of the overburden is large, so the surface well protection devices for non-uniform crush deformation can be positioned at this point.

4.2 Safety protection of the well structure

The safety protection of the wellbore structure in the mining area was mainly achieved on the basis of the following three types of overburden movement conditions: 1) The motions of the overlying strata in the stope were mainly composed of interlayer shear slip,

TABLE 5 Installation parameters for the surface well protection devices.

Serial number	Lithology	Above coal seam/m	Depth/m	Layer thickness/m	Type of protective device	Installation position
1	Coarse-grained sandstone	342.58	69.2	14.40	Thick-walled rigid device	Inside key layer x
2	Siltstone	235.03	176.75	13.30	Stretching guard device	Lower part of key layer VI
3	Medium-grained sandstone	146.43	265.35	9.00	Deflection guard device	Lower part of key layer IV
4	Siltstone	71.15	340.63	8.2	Deflection guard device	Interface between key layer III and lower rock stratum
5	Coarse-grained sandstone	23.00	388.78	13.24	Thick-walled rigid device	Upper part of key layer II

TABLE 6 Deformation monitoring results of the YCCD-04 surface well.

Serial number	Location of the working face and surface well (m)	Surface well deformation
1	21.5 m from the surface well	No obvious deformation of the surface well is detected
2	Pushed 6.8 m over the surface well	No obvious deformation of the surface well is detected
3	Pushed 25 m over the surface well	Starting from 72.3 m above the coal seam, the length of the shear deformation section is approximately 0.45 m and the shear deformation is approximately 0.16 m, indicating that the fracture of key layer III causes shear deformation of the surface well
4	Pushed 60.1 m over the surface well	A small deformation occurred in the surface well 357 m above the coal seam, and cracks were found in the casing of the surface well. The deformation was blocked when the casing was lowered to 78.4 m above the coal seam
5	Pushed 102.2 m over the surface well	A small shear deformation occurred in the surface well 385 m above the coal seam and was seriously deformed at a point 357 m above the coal seam such that the probe could not be lowered. The iron roller rope exploration well was lowered to 25 m above the coal seam, which shows that although the surface shaft is deformed in many places, there is still a certain annular diameter.
6	Pushed 145 m over the surface well	A small deformation occurred at 398.2–400 m above the coal seam. There was a gap in the surface well 384.4–385 m above the coal seam, indicating that damage occurred. Shear deformation occurred in the surface well 357 m above the coal seam. The exploration rope could not be lowered at a point 139 m above the coal seam

and the interface of the shear deformation was prone to damage. 2) During coal seam mining, apparent out-of-layer displacement occurs in the key layer (or combination of key layers) in the overlying strata of the stope. 3) Surface well casing was prone to non-uniform extrusion deformation in the combined rock beam, where the deformation of the well structure was likely due to two or three forms of integrated damage. Hence, it was necessary to analyze the movement law of the overlying strata as well as inhibit the deformation and damage of the surface well. Three types of mining area surface well structure protection devices were thus developed.

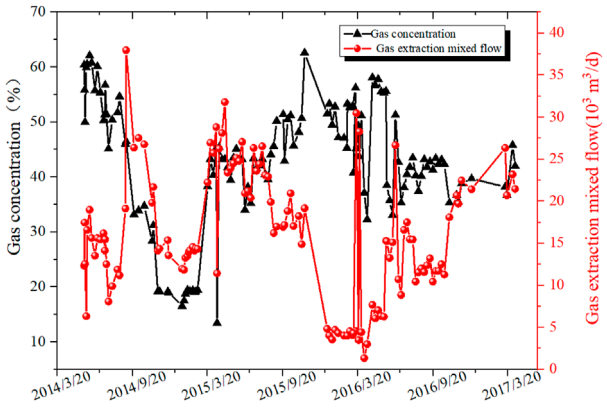

FIGURE 15
Coalbed methane drainage data of the ground coal mine.

4.2.1 Anti-shearing device

Special devices must be installed in the areas where shear failures occur. Therefore, when the rock is cut between the strata, the structural device can move along the sliding direction of the upper and lower rock strata. The occurrence of a certain degree of deviation weakens the rock surface shear on the rigid damage of the original casing. Therefore, the surface well casing deflection structure is meant to allow the structure to move in any direction with a certain degree of deflection. The design of the deflection structure takes into account the limited voids between the well casing and open hole. The deflection angle of the deflection structure in any direction was 3°30'. The deflection structure parameters matching the 244.5-mm N80 oil casing are presented in Table 1. The surface well deflection device mainly includes a rotary head, a rotary sleeve, a screw cover, a gland, a seal, an "O" ring, and six other parts. The assembly diagram and picture of the surface well casing deflection protection device is presented in Figure 10.

4.2.2 Anti-tensile damage device

To prevent any impact of mining on the surface well casing caused by the layer of tensile damage, security devices were installed in parts prone to tensile damage. When an abscission layer occurs between the overlying strata, the antitensile damage device produces a certain amount of expansion in the abscission layer that could weaken the rigid deformation of the casing. The telescopic device for the surface well casing allows elongation in the axial direction. Based on theoretical and critical layer analyses of the key and subkey layers of the 3$^{\#}$coal seam of the Jincheng mining area, the tensile amount of the antitension device was designed to be measured at 300 mm. The parameters of the telescopic device are presented in Table 2.

The surface well antitension device mainly includes a telescopic outer tube, a telescopic inner tube, a guide sleeve, a safety pin, an "O" ring, and five other parts. The telescopic device assembly diagram and picture of the retractable protective device of the surface well casing are presented in Figure 11. Prior to installation of the protective devices, it is necessary to determine the high-risk positions based on the detailed information of the stratum. Accordingly, the protective devices are installed in the determined rock strata.

4.2.3 Thick-walled rigid device

A thick-walled rigid guard was installed at a location where the casing was not uniformly extruded. When placed between the extrusion damage regions in the rock, the thick-walled rigid device can resist most of the impacts on the combined rock beam within the extrusion force to ensure smooth flow of CBM. The parameters for the thick-walled rigid device design are presented in Table 3. According to the casing protection requirements, the length of the thick-walled rigid protective structure could be taken as the following three standard values, namely 2 m, 4 m, and 6 m. The ends and corner parts of the protective structures should be rounded to eliminate stress concentration. The assembly diagram and picture of the thick-walled rigid guards are presented in Figure 12.

5 Engineering practice

5.1 Engineering background

The Qinshui Coalfield in Shanxi province is one of the main bases for coalbed gas development in China, and the Yuecheng Mine considered in this study belongs to the Qinshui Coalfield. In the Shanxi Coal Mine Group, the engineers of the Yuecheng Mine company have designed 10 surface wells in the mining areas. The coal mine utilizes layered mining integrated with mechanical coal mining. The first mining was conducted on the stratification, and subsequent mining efforts were under the stratification. The mining of the working face of the northern part of Yuecheng Mine was in the following order: 1301 (upper), 1302 (upper), 1303 (upper), 1304 (upper), 1301 (lower), 1302 (lower), 1303 (lower), 1304 (lower), 1305 (lower). A part of the well layout of this mine is presented in Figure 13A. The orientation length of the working face in the northern part of the Yuecheng Coal Mine was 170 m, the strike length was 1,100 m, and the average progress of coal mining was 3 m/d. During mining, the gas emission rates are often higher, and the upper limit of the gas concentration is often overrun. The conventional technology of underground CBM drainage cannot control the gas adequately, so it was deemed a good idea to move the surface well to the coal mining face. Considering the 1303 fully mechanized coal mining face in the Yuecheng Mine as an example in this paper, the CBM drainage technology using surface wells under mining was introduced.

The 1303 fully mechanized coal mining face of the Yuecheng Mine was located in Zhaozhuang Village east, which is 606 m northeast of Ling Village. The total thickness of the main coal mining area was 6.20–6.49 m, average thickness was 6.34 m, and average dip angle of the coal seam was 3°. Using the stratified mining method, the first mining was conducted on the stratification (3.2 m) and then continued under the stratification (2.9 m). In the mine, all caving methods were used to manage the roof. The coal dust was not explosive and not prone to spontaneous combustion.

5.2 Deformation and damage monitoring of the surface wells

5.2.1 Monitoring equipment

The Jl-IDOI intelligent well TV imager is applicable to engineering geology, hydrogeology, geological prospecting,

TABLE 7 Gas changes following surface well operations.

Project	Upper limit of gas concentration (%)	Return airway gas concentration (%)	Working face gas emission (m^3/min)
Normal extraction	0.50	0.80	8.24
After the surface well are extracted	0.22	0.33	3.399

geotechnical engineering, mining, oil and CBM development, and other research efforts. Advanced digital image acquisition and signal processing technologies, high system integration, probe panoramic camera, real-time automatic section extraction, clear and realistic images, automatic and accurate calibration of the azimuth and depth, and all-round and all-cylindrical monitoring and imaging of all observation holes were adopted. The equipment comprised transmission cables, high-definition displays, detection probes, tripods, and fixed wheels. The probe types and relative parameters of the well imager are shown in Table 4.

According to the overburden characteristics of the test mining area, we determined the detection time requirements of the surface well imager and monitored the deformation and damage of the surface well under the conditions that the working face was 45 m, 30 m, 20 m, 10 m, and 0 m away from the surface well as well as 10 m, 20 m, 30 m, 45 m, 60 m, 80 m, 110 m, 150 m, and 200 m away from the surface well. The deformation site detection using the well imager in the surface well is shown in Figure 14.

5.2.2 Deformation and damage of surface wells without protective devices

To verify the effectiveness of using protective devices against deformation and damage of mining gas drainage surface wells in the Jincheng mining area, we detected the deformation and damage of the YCCD-04 and YCCD-02 wells in the Yuecheng Coal Mine using a surface well imager to analyze the drainage effect on repeated mining gas surface wells. We also compared the deformation of a surface well with protection devices (YCCD-02) to that without any protection devices (YCCD-04).

In the downhole casing of the YCCD-02 well, tensile protection devices were installed between the key and lower layers, antideflection protection devices were installed in the rock layer with alternating soft and hard thickness, and thick-walled rigid protection devices were installed in the composite rock beam. The installation positions are shown in Table 5. The influence from mining will cause deformation of the surface well casing and even damage. The deformation and failure process obtained by monitoring the YCCD-04 well during the upper-layer recovery are shown in Table 6 and Figure 14. By analyzing the casing deformation of the YCCD-04 well in the Yuecheng Coal Mine, it was found that the surface well was not obviously deformed or damaged before the working face reached the surface well. As the working face advanced through the surface well, the deformation of the well gradually expanded from bottom to top, and the deformation and damage degree of the surface well intensified with advancement of the working face. Thus, the YCCD-04 surface well failed for successful gas extraction.

5.3 Gas drainage effects of surface wells with protective devices

Protective devices were installed in the Shanxi Coal Group Yuecheng Mine, in which ten surface wells were constructed in the mining area; the YCCD-02 surface well was considered as the example in this case. The surface well was near the 1303 working face of Yuecheng Mine at distances of 700 m from the cutting hole and 35 m from the return airway; the length of the working face was 158 m. The two adjacent working face pillars had widths of 30 m each. When the 1303 working face was mined, a large-sized crack conduction space and high quantity of CBM was found within. The body structures of the three open wells were situated at depths of 50 m and had J55-type casings. At the second opening, the depth was 308 m, and the N80 casing was used for partial cementing at a depth of 95 m from the surface. At the two openings, antishear, anti-non-uniform extrusion, and antistretching protection devices were installed at depths of 148 m, 205 m, 255.4 m, and 298 m. At the third opening at a depth of 394 m, the coal seam had a penetration of 10 m, and three open screen pipes were located 5 m above the coal seam.

CBM extraction in the YCCD-02 surface well in the mining-affected area began on 25 May 2014. When the coal seam was under stratified mining, the maximum CBM extraction was 3.79 $\times$ 10^4 m^3/d, average drainage capacity of the surface well was 1.15 $\times$ 10^4 m^3/d, maximum CBM concentration was 62.6%, average coal-seam gas concentration was 42.42%, extraction duration was 35 months, and cumulative pumping was approximately 1.3 $\times$ 10^7 m^3 of gas; the pumping data are presented in Figure 15. Subsequent to CBM drainage through the surface well in the mining area, the return airway gas concentration at the mining working face decreased by 58.75%, while the average return airway gas concentration was only 0.33%. The gas concentrations at the upper limit and return airway of the working face decreased significantly, while the safety of the goaf was effectively eliminated, as shown in Table 7.

In the present study, the extraction of coalbed gas through the surface well in the mining area was analyzed, and certain technical details that required further improvement were identified. The movements of the overlying strata had large effects on the casing of the surface well, while the movement law of the overlying rocks and its effects on the surface well were significantly complicated. The next step would therefore be an in-depth study of the impacts of coal mining on the surface well in the mining area. Moreover, protection devices play important roles in the local safety of the surface wells. Flexible safety protection devices should be developed to improve the stabilities of the surface wells. In addition, according to the theoretical calculations and analyses, when the casing size of the surface well was larger, then the casing wall thickness was larger, steel

grade was higher, and surface well deformation was increasingly difficult. However, larger surface well diameters can result in greater difficulty of surface well drilling. The higher the casing wall thickness and steel grade, the higher is the cost of the surface well. Therefore, it is necessary to develop a suitable surface well structure to solve these problems.

6 Conclusion

The present study analyzes the key technologies required for surface wells in the longwall working face under mining effects to ensure smooth extraction of CBM as well as coal mine safety. The deformation model of the overlying strata was established to analyze the separation, shear, and non-uniform extrusion deformation characteristics. Three types of safety protection devices were developed for the antitensile, antishear, and anti-non-uniform extrusion damages of the surface well. The approach involved optimization of the surface well structure and identification of the locations that would make the surface wells vulnerable to damage so that protective devices could be installed. Several conclusions can be drawn from the findings of this study:

(1) Based on the characteristics of the stope roof cracks and gas flow in the overlying strata, the basic principles regarding the surface well layout were obtained. Surface wells should be located as far as possible from the areas of maximum shear and delamination stretching. Moreover, the surface wells should be located between the surface settlement and midline.

(2) In the Yuecheng Coal Mine of the Jincheng mining area, several surface wells are used for drainage of the mining gas. The YCCD-04 well without any local protective devices was deformed and damaged, and the dynamic deformation and failure process of this surface well was detected using a well imager. The YCCD-02 well that has installed local protective devices showed good mining and gas drainage effects, thus verifying the effectiveness of local protective devices.

(3) The CBM drainage duration of the YCCD-02 well was approximately 35 months, with the highest CBM drainage volume being 3.79×10^4 m^3/d and cumulative volume of CBM drainage being 1.31×10^7 m^3. This solved the problem of gas control in the overlying strata and ensured safety during the coal mining operations.

Author contributions

JF: conceptualization, funding acquisition, methodology, validation, and writing–original draft. GW: conceptualization, project administration, supervision, and writing–review and editing. BZ: software and writing–review and editing. HS: investigation, resources, and writing–review and editing. RL: data curation, funding acquisition, and writing–review and editing. JL: formal analysis, visualization, and writing–review and editing.

Funding

The authors declare that financial support was received for the research, authorship, and/or publication of this article. This study was supported by the Chongqing Talent Program Project (no. cstc2022ycjh-bgzxm0021), the Chongqing Natural Science Foundation Project (no. CSTB2022NSCQ-MSX0379), Chongqing Research Institute's Independent Innovation Leading Project (no. 2024YBXM35), and Scientific Research Project of middling coal Science and Engineering Group Chongqing Research Institute Co., Ltd (2024YBXM35).

Conflict of interest

The authors declare that the research was conducted in the absence of any commercial or financial relationships that could be construed as a potential conflict of interest.

The authors declare that this study received funding from Scientific Research Project of middling coal Science and Engineering Group Chongqing Research Institute Co., Ltd. The funder had the following involvement in the study: design, analysis and the writing of this article.

Publisher's note

References

Buzek, F., Cejkova, B., Jackova, I., Gerslova, E., Mach, K., Lhotka, M., et al. (2022). Secondary processes on coal deposits change the emission of greenhouse gases. *Int. J. Coal Geol.* 262, 104102. doi:10.1016/j.coal.2022.104102

Chen, W., Li, W., He, J., Qiao, W., Wang, Q., and Yang, Y. (2022). Impact of mining-induced bed separation spaces on a cretaceous aquifer: a case study of the Yingpanhao coal mine, Ordos Basin, China. *Hydrogeology J.* 30 (2), 691–706. doi:10.1007/s10040-022-02455-y

Chi, M., Zhang, D., Liu, H., Wang, H., Zhou, Y., Zhang, S., et al. (2019). Simulation analysis of water resource damage feature and development degree of mining-induced fracture at ecologically fragile mining area [Article]. *Environ. Earth Sci.* 78 (3), 88. doi:10.1007/s12665-018-8039-5

Fu, J., Sun, H., Wen, G., and Li, R. (2020). Three-dimensional physical similarity simulation of the deformation and failure of a gas extraction surface well in a mining area. *Adv. Civ. Eng.* 2020, 8834199. doi:10.1155/2020/8834199

Guo, B., Li, Y., Jiao, F., Luo, T., and Ma, Q. (2018). Experimental study on coal and gas outburst and the variation characteristics of gas pressure. *Geomechanics Geophys. Geo-Energy Geo-Resources* 4 (4), 355–368. doi:10.1007/s40948-018-0092-8

Jha, P., Ghosh, S., Vidyarthi, A. S., Singh, J., Mukhopadhyay, K., and Prasad, R. (2022). Unravelling the microbial community structure and function of coal-bed methane producing formation water of Jharia coal mines using metagenomics approach. *Fuel* 317, 123459. doi:10.1016/j.fuel.2022.123459

Joshi, D., Prajapati, P., Sharma, P., and Sharma, A. (2023). Past, present and future of Coal Bed Methane (CBM): a review with special focus on the Indian scenario. *Int. J. Coal Prep. Util.* 43 (2), 377–402. doi:10.1080/19392699.2022.2051014

Ju, Y., Wang, Y., Su, C., Zhang, D., and Ren, Z. (2019). Numerical analysis of the dynamic evolution of mining-induced stresses and fractures in multilayered rock strata using continuum-based discrete element methods. *Int. J. Rock Mech. Min. Sci.* 113, 191–210. doi:10.1016/j.ijrmms.2018.11.014

Kishor, K., Kumar Srivastava, M., and Singh, A. K. (2023). Geochemical study of coals from Sohagpur Coalfield, India, and its implication to CBM potential. *Int. J. Coal Prep. Util.* 44 (6), 614–625. doi:10.1080/19392699.2023.2212611

Kong, S., Cheng, Y., Ren, T., and Liu, H. (2014). A sequential approach to control gas for the extraction of multi-gassy coal seams from traditional gas well drainage to mining-induced stress relief. *Appl. Energy* 131, 67–78. doi:10.1016/j.apenergy.2014.06.015

Li, L., Tang, J., Sun, S., and Ding, J. (2019). Experimental study of the influence of water content on energy conversion of coal and gas outburst. *Nat. Hazards* 97 (3), 1083–1097. doi:10.1007/s11069-019-03687-0

Liu, Y., Lu, T., and Yu, H. (2005). Surface boreholes for drainage of goaf gases and its stability analysis. *Rock Mech. Eng.* 24 (Suppl. L.), 4987.

Luan, Y., Dong, Y., Ma, Y., and Weng, L. (2020). Surface and new building deformation analysis of deep well strip mining. *Adv. Mater. Sci. Eng.* 2020, 8727956. doi:10.1155/2020/8727956

Newman, C., Agioutantis, Z., and Leon, G. B. J. (2017). Assessment of potential impacts to surface and subsurface water bodies due to longwall mining [Article]. *Int. J. Min. Sci. Technol.* 27 (1), 57–64. doi:10.1016/j.ijmst.2016.11.016

Ponnudurai, V., Kumar, P. S., Muthuvelu, K. S., Velmurugan, S., Subhani, S., Arumugam, L., et al. (2022). Investigation on future perspectives of *ex-situ* biogenic methane generation from solid waste coal and coal washery rejects [Article]. *Fuel* 318, 123497. doi:10.1016/j.fuel.2022.123497

Qu, Q., Guo, H., and Loney, M. (2016). Analysis of longwall goaf gas drainage trials with surface directional boreholes. *Int. J. Coal Geol.* 156, 59–73. doi:10.1016/j.coal.2016.02.001

Ran, Q., Liang, Y., Zou, Q., Zhang, B., Li, R., Chen, Z., et al. (2023). Characteristics of mining-induced fractures under inclined coal seam Group multiple mining and implications for gas migration. *Nat. Resour. Res.* 32 (3), 1481–1501. doi:10.1007/s11053-023-10199-z

Ren, B., Yuan, L., Sang, S., Guo, H., Xue, J., Huang, H., et al. (2018). Deformation and damage of pressure-relieved gas extraction wells in deep mining under thick surface soil and their prevention with Guqiao of Huainan mine as an example. *COAL Geol. and Explor.* 46 (05), 159–166. doi:10.3969/j.issn.1001-1986.2018.05.025

Sang, S. X., Xu, H. J., Fang, L. C., Li, G. J., and Huang, H. Z. (2010). Stress relief coalbed methane drainage by surface vertical wells in China. *Int. J. Coal Geol.* 82 (3-4), 196–203. doi:10.1016/j.coal.2009.10.016

Schatzel, S. J., Karacan, C. O., Dougherty, H., and Goodman, G. V. R. (2012). An analysis of reservoir conditions and responses in longwall panel overburden during mining and its effect on gob gas well performance. *Eng. Geol.* 127, 65–74. doi:10.1016/j.enggeo.2012.01.002

Su, W. H., Zhang, P., Dougherty, H., Van Dyke, M., Minoski, T., Schatzel, S., et al. (2019). Longwall mining, shale gas production, and underground miner safety and health. *Int. J. Min. Sci. Technol.* 31 (3), 523–529. doi:10.1016/j.ijmst.2020.12.013

Sun, Z., Xu, S., Jiao, J., Wang, S., To, S., and Li, P. (2022). Surface deformation errors and self-adaptive compensation for microstructured surface generation of titanium alloys. *Int. J. Mech. Sci.* 236, 107736. doi:10.1016/j.ijmecsci.2022.107736

Wang, L., Cheng, Y.-p., An, F.-h., Zhou, H.-x., Kong, S.-l., and Wang, W. (2014). Characteristics of gas disaster in the Huaibei coalfield and its control and development technologies. *Nat. Hazards* 71 (1), 85–107. doi:10.1007/s11069-013-0901-x

Wang, P., Jiang, J., and Xu, B. (2020). Breaking and instability movement characteristics of high-position double-layer hard thick strata due to longwall mining [article]. *Shock Vib.* 2020, 8887026. doi:10.1155/2020/8887026

Wang, Y., Fan, X., Niu, K., and Shi, G. (2019). Estimation of hydrogen release and conversion in coal-bed methane from roof extraction in mine goaf. *Int. J. Hydrogen Energy* 44 (30), 15997–16003. doi:10.1016/j.ijhydene.2019.01.152

Whittles, D. N., Lowndes, I. S., Kingman, S. W., Yates, C., and Jobling, S. (2006). Influence of geotechnical factors on gas flow experienced in a UK longwall coal mine panel. *Int. J. Rock Mech. Min. Sci.* 43 (3), 369–387. doi:10.1016/j.ijrmms.2005.07.006

Whittles, D. N., Lowndes, I. S., Kingman, S. W., Yates, C., and Jobling, S. (2007). The stability of methane capture boreholes around a long wall coal panel. *Int. J. Coal Geol.* 71 (2), 313–328. doi:10.1016/j.coal.2006.11.004

Xu, H. J., Sang, S. X., Fang, L. C., and Huang, H. Z. (2011). Production characteristics and the control factors of surface wells for relieved methane drainage in the huainan mining area. *Acta Geol. Sinica-English Ed.* 85 (4), 932–941. doi:10.1111/j.1755-6724.2011.00496.x

Ye, Q., Li, C., Yang, T., Wang, Y., Li, Z., and Yin, Y. (2023). Relationship between desorption amount and temperature variation in the process of coal gas desorption. *Fuel* 332, 126146. doi:10.1016/j.fuel.2022.126146

Zhang, B., Liang, Y., Sun, H., Wang, K., Zou, Q., and Dai, J. (2022). Evolution of mining-induced fractured zone height above a mined panel in longwall coal mining. *Arabian J. Geosciences* 15, 476. doi:10.1007/s12517-022-09768-y

Zhang, B., Sun, H., Liang, Y., Wang, K., and Zou, Q. (2020a). Characterization and quantification of mining-induced fractures in overlying strata: implications for coalbed methane drainage. *Nat. Resour. Res.* 29, 2467–2480. doi:10.1007/s11053-019-09600-7

Zhang, B. C., Liang, Y. P., Zou, Q. L., Ning, Y. H., and Kong, F. J. (2024). Damage and hardening evolution characteristics of sandstone under multilevel creep-fatigue loading. *Geomechanics Geophys. Geo-Energy Geo-Resources* 10 (1), 43. doi:10.1007/s40948-024-00751-3

Zhang, K., Bai, L., Wang, P., and Zhu, Z. (2021). Field measurement and numerical modelling study on mining-induced subsidence in a typical underground mining area of northwestern China. *Adv. Civ. Eng.* 2021, 5599925. doi:10.1155/2021/5599925

Zhang, P., Su, D., Van Dyke, M., and Kim, B. H. (2023). *A case study of shale gas well casing deformation in longwall chain pillars under deep cover 57th U.S. Rock Mechanics Geomechanics Symposium*. Atlanta, GA.

Zhang, Z., Deng, M., Wang, X., Yu, W., Zhang, F., and Dao, V. D. (2020b). Field and numerical investigations on the lower coal seam entry failure analysis under the remnant pillar. *Eng. Fail. Anal.* 115, 104638. doi:10.1016/j.engfailanal.2020.104638

Zhao, P., Zhuo, R., Li, S., Shu, C., Jia, Y., Lin, H., et al. (2021). Fractal characteristics of methane migration channels in inclined coal seams. *Energy* 225, 120127. doi:10.1016/j.energy.2021.120127

Zhou, A., Hu, J., and Wang, K. (2020). Carbon emission assessment and control measures for coal mining in China. *Environ. Earth Sci.* 79 (19), 461. doi:10.1007/s12665-020-09189-8

Zhuo, R., Zhao, P., Li, S., Lin, H., Liu, H., Kong, X., et al. (2024). Effects of coal thickness on the fractal dimension of gas migration channels: laboratory and field study of a gassy coal mine. *Nat. Resour. Res.* 33 (3), 1193–1208. doi:10.1007/s11053-024-10330-8